Energy-Resolved Neutron Technique for Metal Material Analysis

Junyoung Son [a], Daeseung Kim [a], Yumin Heo [a], Junhyeok Won [a], Seungwook Lee [a*]
[a]*School of Mechanical Engineering, Pusan National University, Busan 46241, South Korea*
**Corresponding author: seunglee@pusan.ac.kr*

1. Introduction

In the field of material analysis, using neutrons is one of the important techniques. There are various methods of analysis using neutrons, neutron transmission for observing the internal structure of materials and neutron diffraction analysis for obtaining crystallographic information are representative. Neutron transmission can measure a wide area but does not include crystallographic information. On the other hand, neutron diffraction analysis can only measure a limited area but can analyze crystallographic information [1]. The proposed method in this study is an imaging method using energy-resolved neutrons that complement wide area and crystallographic information as a solution to overcome these disadvantages of limited area and insufficient crystallographic information. This study includes a preliminary study to determine the crystal lattice distance (d-spacing) according to uniaxial deformation of pure Fe (99.99 %) sample and to obtain crystallographic information such as crystal structure factor through diffraction pattern for later study.

2. Methods

2.1 Neutron Transmission

The Beer-Lambert law is used to obtain contrast information based on the degree of total attenuation for independent object characterization in transmission imaging [2]. By dividing the incident neutron beam, $I0$, and the transmitted neutron beam, I, a contrast value between 0~1 can be obtained. In this study, the transmission characteristics of each pixel are utilized, and the presence of dark current and constant background noise before image processing is assumed to follow a Poisson distribution in all images. To improve image quality, dark current was removed prior to image processing.

$$Tr = \frac{I-DC}{I_0-DC} = e^{-\mu_{tot}t} \quad (1)$$

The incident neutrons are represented by I_0, while I represents the neutrons after passing through the object. total linear attenuation factor, μ_{tot}, takes into account the characteristics of the object and the incident beam. The thickness of the object is represented by t.

2.2 Bragg's law

Like X-rays, neutrons demonstrate diffraction and reflection properties that can be explained by Bragg's law, physical principle.

$$\lambda = 2d_{hkl}sin\theta \quad (2)$$

where λ is the wavelength of the neutron, d_{hkl} is the d-spacing of the crystal lattice plane {hkl}, and θ is the Bragg angle for the crystal lattice plane.

Neutron diffraction angles with crystal lattice planes depend on wavelength, with a maximum at 90° for $\lambda=2d_{hkl}$. Crystal structures are not arranged in just one direction, resulting in different crystal groups aligned differently. Diffraction occurs at a shorter wavelength than $2d_{hkl}$ when the angle between the incident beam and the crystal lattice plane is not perpendicular. Coherent elastic scattering does not take place when the incident neutron wavelength is longer than $2d_{hkl}$. Traditional neutron imaging systems utilize continuous energy beams and cannot arrange crystals in a single direction, leading to a mixture of diffracted wavelengths. To overcome this problem and effectively categorize and utilize the diffraction phenomena, it is necessary to decompose the detected wavelengths and take into account the presence of multiple crystal phase [3].

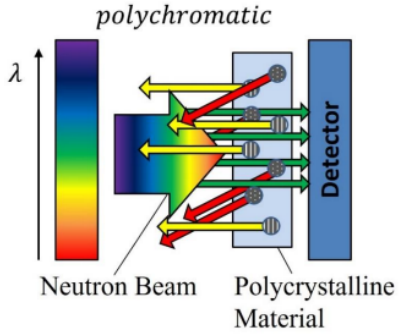

Fig. 1. A scheme of polychromatic beam elastic scattering of polycrystalline materials.

2.3 Time of Flight

The time-of-flight (TOF) method is a technique used to distinguish between different energies or wavelengths by measuring the distance traveled by a particle or wave and the amount of time it takes to do so. In a neutron imaging system, neutron source and detector are positioned in a straight line. If the neutron generation takes place at regular period and the detector can measure these neutrons at the specific time gap, the wavelength of

the neutrons can be calculated using the following equation.

$$\lambda = \frac{h}{p} = \frac{h}{mv} = \frac{h(\Delta t - t_0)}{mL} \quad (3)$$

Where λ is neutron wavelength, h is the Planck constant, m is the mass of the neutron (ignoring the relativistic mass due to the small energy), L is the distance between the neutron generation point and the detector, and Δt and t_0 represent the difference between the generation time and measurement time of the neutron. With the help of a detector with time resolution and by taking into account the distance of the detection system, the wavelength of the neutron can be distinguished.

2.4 Wavelength Dependent Transmission Imaging

Wavelength-dependent transmission images can be created by utilizing the transmission properties of neutrons and the diffraction properties described by Bragg's law at specific lattice distance. At this time, the collected images using neutrons contain crystallographic information such as preferred orientation, crystal lattice distance, phase distribution, and texture. Neutrons that pass through the material generate a Bragg pattern signal that varies with a specific wavelength, and when this collected pattern signal is divided by the neutron signal prior to passing through the material, only the Bragg pattern that varies with wavelength remains. This signal depends on the total cross section of the material in the cold neutron region, which expressed as the coherent elastic scattering, incoherent elastic scattering, coherent inelastic scattering, incoherent inelastic scattering, and absorption cross-section as: [4, 5]

$$\sigma_{tot}(\lambda) = \sigma_{coh}^{eal}(\lambda) + \sigma_{incoh}^{eal}(\lambda) + \sigma_{coh}^{ineal}(\lambda) + \sigma_{incoh}^{ineal}(\lambda) + \sigma_{abs}(\lambda), \quad (4)$$

The coherent elastic scattering can be expressed as:

$$\sigma_{coh}^{eal}(\lambda) = \frac{\lambda^2}{2V_0}\sum_{d_{hkl}=0}^{2d_{hkl}<\lambda}|F_{hkl}|^2 d_{hkl} B_{hkl}(\lambda, d_{hkl}) P_{hkl}(\alpha_{hkl}(\lambda)) Ext(\lambda, S), \quad (5)$$

V_0 is the volume of the unit crystal, d_{hkl} is the crystal lattice spacing for the Miller index hkl, F_{hkl} is the crystal structure factor including the Debye-Waller factor. B_{hkl} is broadening of the Bragg-edge due to the neutron pulse width in the case of pulsed neutrons, represents a resolution function that describes the neutron irradiation environment of the facility. P_{hkl} and α_{hkl} are functions to include the preferred orientation, and Ext is a function for re-diffraction or transmission that occurs depending on the crystal size and grain size. The simulations were performed using Rits[4, 5] codes.

2.5 Facility

The experiment was carried out at the Hokkaido University Neutron Source (HUNS) in Japan, using a pulsed cold neutron beamline based on the accelerator (LINAC-II). the beam line is 6.24 m. And A GEM-type TOF detector is 128 x 128 pixels, each 800 μm in size. To reduce errors in the data by non-parallel neutron scattering, a grid-type collimator made of Gd_2O_3 and aluminum was installed in front of the detector. This collimator absorbed neutrons coming from unpreferred directions, increasing the angular dependence of neutrons. A collimator measuring 10 cm x 10 cm was used to achieve this in the experiment.

2.5 Samples

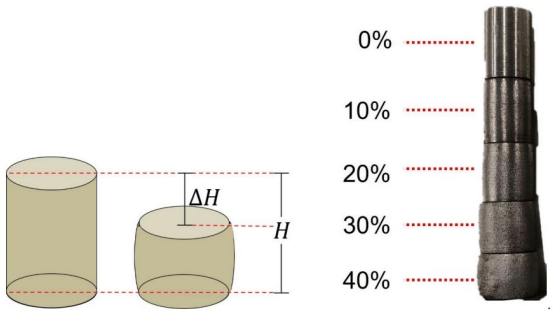

Fig. 2. Sample deformation method and pictures of each compressed sample.

Five cylindrical specimens with a height of 15 mm and a diameter of 10 mm were produced using pure iron (Fe99.9%) to minimize the influence of other elements and best represent the ferrite structure. Water cutting was used to minimize structural deformation during the cutting process. Uniaxial compression tests were conducted using a hydraulic press to evaluate external and internal deformation at 10%, 20%, 30%, and 40% compression ratios, as described by reference. The calculation of the external strain is as follows.

$$\varepsilon_{ex} = \frac{\Delta H}{H} \quad (6)$$

3. Results

A total of 1429 time-of-flight images were collected at intervals of 10 μs, and the wavelength was determined based on the distance between the source and detector. By displaying the image pixel by pixel at the calculated wavelength, information on the edge pattern of the sample at each pixel location was obtained. To reduce statistical errors caused by the small number of neutrons, the values were averaged using a median filter and the nearest neighboring pixels on the x and y axes. This approach may result in some blurring of the spatial resolution, but it does not significantly affect the position of the peak, which is wavelength-dependent. It is determined that the increase in the transmittance ratio is due to the increase in the thickness due to the spread of

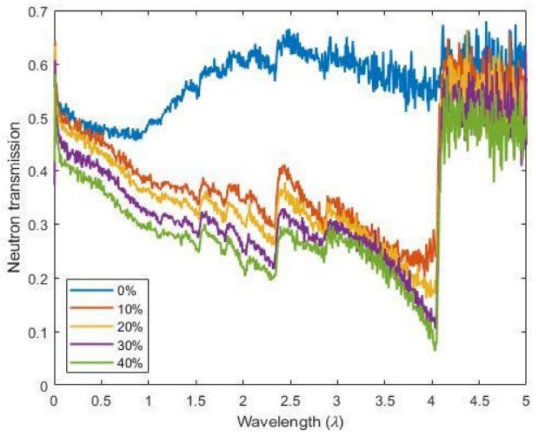

Fig. 3. The patterns obtained for each sample at different wavelengths.

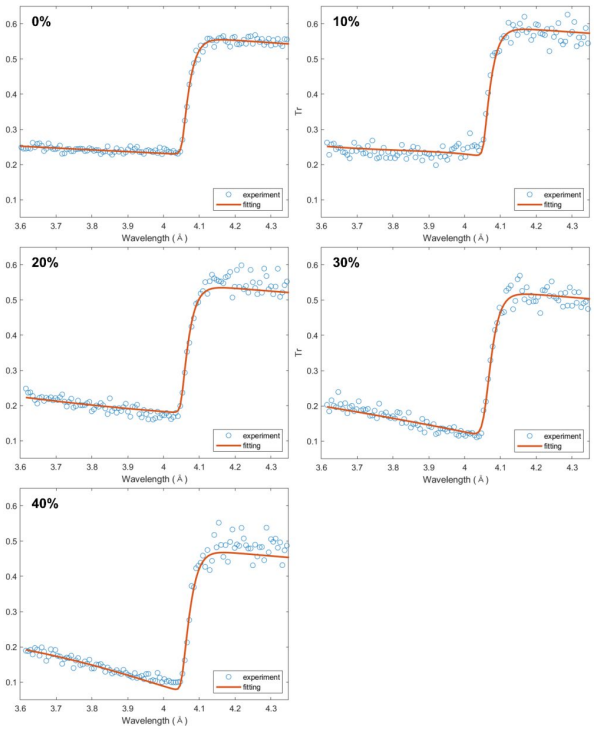

Fig. 4. (110) crystal plane single edge fitting of 0%, 10%, 20%, 30%, 40% compression specimens.

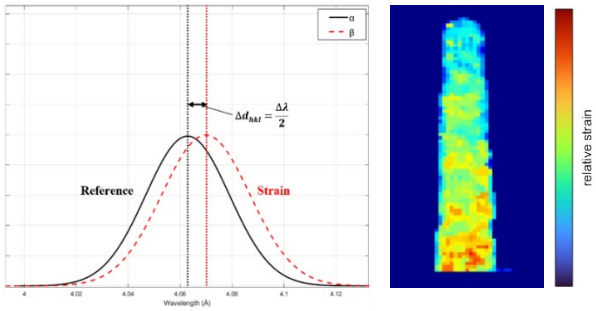

Fig. 5. Difference in crystal lattice distance before and after deformation through Gaussian fitting (left) and Relative strain mapping image. (right)

the sample in the direction perpendicular to the direction of the force in uniaxial compression. And it was confirmed that the position of 4 Å, that is, the shape of the peak around the BCC (110) plane changes as the external strain is stronger. This is caused by a change in the diffraction that occurs depending on the preferred orientation of the crystal lattice or the number of grains in the sample. The shape of the peak tends to deepen according to the degree of compression of the sample, and it can be confirmed that the arrangement of the crystal lattice becomes homogeneous according to the degree of compression during the compression process. In the 0% sample, a peculiar flow can be seen. If the size of the crystal with the crystal planes arranged in the same direction is relatively large, it can be inferred that the diffracted neutrons are diffracted again and enter the detector to increase the transmittance. Finally, the left-right movement of the peak means the change of the diffracted crystal lattice plane distance [6]. Through this, the internal deformation in the material was evaluated. The expression for the internal strain is.

$$\varepsilon_{in} = \frac{d-d_0}{d_0} \tag{7}$$

d is the position of the shifted peak and d_0 is the position of the peak before strain. To determine the peak of the edge point, the midpoint of the change was calculated using Gaussian fitting at the differential of the edge pattern. The shift of the peak point is the change of the diffracted wavelength, indicating the average distance of the crystal lattice. The spread of the Gaussian function reflects the fine and diverse distribution of the crystal lattice, while the central point of the peak represents the average strain. To assess the sample's strain, single edge fitting was performed in the [110] lattice structure region. The fitting process was conducted using RITS software and MATLAB. The average strains for the 10%, 20%, 30%, and 40% samples were 93 με, 212 με, 329 με, and 409 με, respectively, calculated by fitting each sample pixel by pixel. The average internal strain was observed to change in accordance with the external strain and could be visually verified by mapping the average strain data onto an image.

4. Conclusions

We conducted an analysis using energy-resolved neutrons, which combines the benefits of neutron transmission imaging and neutron diffraction analysis. We observed a Bragg-edge pattern that varies with wavelength and derived the average crystal lattice distance for each sample with different strain, indicating their average degree of strain. Moreover, we confirmed that the average internal strain increased proportionally to the external strain. Our study confirms the possibility of non-destructive material analysis using neutrons, even in a relatively small laboratory-scale accelerator-based

pulsed neutron facility, without relying on a large research reactor or spallation neutron facility. Future studies will investigate additional structural parameters.

ACKNOWLEDGEMENTS

This work was supported by the National Research Institute of Cultural Heritage grant funded by the Cultural Heritage Administration (No. 2021A01D03-001).

REFERENCES

[1] H. Sato, Quantitative imaging of crystalline structural information by pulsed neutron transmission, Hamon, vol. 22, no. 2, pp. 156-161, 2012.
[2] W. H. Bragg and W. L. Bragg, The reflection of X-rays by crystals, Proceedings of the Royal Society of London. Series A, Containing Papers of a Mathematical and Physical Character, vol. 88, no. 605, pp. 428-438, 1913.
[3] Woracek, Robin, Energy selective neutron imaging for the characterization of polycrystalline materials, PhD diss., University of Tennessee, 2015.
[4] H. Sato, T. Kamiyama and Y. Kiyanagi, A Rietveld-Type Analysis Code for Pulsed Neutron Bragg-Edge Transmission Imaging and Quantitative Evaluation of Texture and Microstructure of a Welded α-Iron Plate, Materials Transactions, Vol. 52, no. 6, pp. 1294-1302, 2011
[5] H. Sato, K. Watanabe, K. Kiyokawa, R. Kiyanagi, K. Y. Hara, T. Kamiyama, M. Furusaka, T. Shinohara and Y. Kiyanagi, Further Improvement of the RITS Code for Pulsed Neutron Bragg-edge Transmission Imaging, Physics Procedia, Vol 88, pp. 322-330, 2017.
[6] J. R. Santisteban et al., Strain imaging by Bragg edge neutron transmission, Nuclear Instruments and Methods in Physics Research Section A: Accelerators, Spectrometers, Detectors and Associated Equipment, vol. 481, no. 1, pp. 765-768, 2002.